International Journal of Heat and Mass Transfer 68 (2014) 500–508

Contents lists available at ScienceDirect

International Journal of Heat and Mass Transfer

journal homepage: www.elsevier.com/locate/ijhmt

Vaporization of two liquid oxygen (LOX) droplets in tandem in convective hydrogen streams at supercritical pressures

Hua Meng [a], Vigor Yang [b,*]

[a] School of Aeronautics and Astronautics, Zhejiang University, Hangzhou, Zhejiang 310027, China
[b] Daniel Guggenheim School of Aerospace Engineering, Georgia Institute of Technology, Atlanta, GA 30332, USA

ARTICLE INFO

Article history:
Received 7 July 2013
Received in revised form 16 September 2013
Accepted 18 September 2013
Available online 18 October 2013

Keywords:
Supercritical fluids
Droplet vaporization
Droplet interaction
Two droplets in tandem

ABSTRACT

Vaporization of two liquid oxygen (LOX) droplets in tandem in supercritical convective hydrogen environments has been numerically investigated. The theoretical formulation consists of a complete set of conservation equations of mass, momentum, energy, and species concentrations. The solution technique is based on a unified treatment of general fluid thermodynamics incorporated into a dual time-stepping preconditioning approach. In addition, a self-consistent property evaluation method is implemented to calculate strong property variations in the transcritical and supercritical fluid regimes. The flow conditions cover a range of pressures between 100 and 400 atm and freestream velocities from 2.5 to 20 m/s. Special attention is given to the effect of droplet interaction on the droplet dynamics and vaporization characteristics. Results indicate that the vaporization behaviors of the two interacting droplets are different from those of an isolated droplet. The presence of the trailing droplet has a minor effect on the lifetime and trajectory of the leading droplet. In contrast, the lifetime of the trailing droplet is substantially prolonged and its moving trajectory is strongly altered. At an ambient pressure of 100 atm, a forward bag-type break-up of the leading droplet is observed when the two droplets are placed closely, with the H/R (the initial droplet spacing to the droplet radius) ratio less than 4. Under the same operating conditions, forward movement takes place for the trailing droplet. Increasing ambient pressure weakens droplet interaction.

1. Introduction

Droplet vaporization and combustion at supercritical pressures play an important role in high-pressure combustion devices such as liquid-propellant rockets, gas turbines, and diesel engines [1]. Many experimental and numerical studies have been conducted in this field over the past decades, mainly focusing on isolated droplets evaporating and burning in quiescent environments [2–14]. These results are pertinent to droplet vaporization in a dilute spray. To comprehend droplet characteristics in a dense spray, effects of droplet interactions on the vaporization process in a quiescent environment have also been examined [15–17].

In practical engine operating conditions, because of fuel injection and strong gas flow motion, droplets generally evaporate and burn in a forced convective environment. The subject has attracted significant research interest [18–22]. Both hydrocarbon fuel droplets evaporating and burning in air (nitrogen) [18,20–22] and liquid oxygen (LOX) droplet vaporization in hydrogen [19] at high pressures have been extensively investigated. Effects of free-stream velocity on droplet lifetime and dynamics have been studied. Correlations of the mass and momentum transfer between the droplet and free stream were established in terms of the droplet thermodynamic state and ambient flow condition [19–22]. The situation in a turbulent flow was also examined [21].

Based on existing data from spray imaging and visualization experiments of the mono-dispersed droplet stream [23–25], it was observed that droplet interactions exert a strong influence on droplet vaporization rates in forced convective environments under both sub- and super-critical fluid conditions. Several numerical studies concerning droplet interaction and vaporization in convective environments have thus been conducted [26–30]. Raju and Sirignano [26] examined two droplets moving in tandem at a subcritical pressure over a range of initial Reynolds numbers, droplet spacing, and droplet diameters. Droplet interaction was found to produce strong influence on the vaporization process, and depending on the initial Reynolds number and droplet spacing, the droplets may collide. Chiang et al. [27,28] later investigated a similar problem with consideration of thermophyscial property variations. The drag coefficient was shown to be overestimated by 20% with fluid properties treated as constants. Correlations were obtained for the drag coefficient, and the Nusselt and Sherwood numbers

* Corresponding author.
E-mail address: vigor.yang@aerospace.gatech.edu (V. Yang).

0017-9310/$ - see front matter © 2013 Elsevier Ltd. All rights reserved.
http://dx.doi.org/10.1016/j.ijheatmasstransfer.2013.09.041

Nomenclature

D	droplet diameter
e_t	total internal energy
E, F	convective flux vector
E_v, F_v	diffusive flux vector
H	droplet spacing
m	droplet mass
p	pressure
q	thermal diffusion flux
Q	dependent variable vector
r	coordinate
R	droplet radius
Re	Reynolds number
S	source term vector
t	time
u	velocity
$\hat{u}$	mass diffusion velocity
x	coordinate
Y_i	mass fraction of species i

Greek symbols

μ	viscosity
ρ	density
τ	viscous stress tensor

Subscripts

0	initial quantity
c	critical values
i	species i
r	quantity in r direction
x	quantity in x direction
∞	ambient parameter

for the two interacting droplets. Frackowiak et al. [29] recently conducted a numerical simulation of droplet interaction and evaporation in a mono-dispersed stream. Strong interaction was found to exist between closely spaced droplets in a dense spray, thereby significantly decreasing the heat and mass transfer coefficients between droplets and the ambient gas. They further showed that the Marangoni force is more important than the viscous force in driving the internal motion and influencing the temperature distribution inside droplets. Cho et al. [30] carried out three-dimensional numerical studies on droplet combustion with multiple droplets interacting in a turbulent environment. The spacing between neighboring droplets both in the streamwise and spanwise directions was found to play an important role in dictating the vaporization and burning processes. The effect of turbulence appears to be moderate [31].

All the previous studies concerning droplet interaction and vaporization in forced convective environments were carried out at subcritical pressures. The situation with supercritical pressure, which plays an important role in many practical engine combustors, needs further investigation. In this paper, the interaction and vaporization of two liquid oxygen (LOX) droplets in tandem in a supercritical hydrogen stream are examined systematically. The analysis is based on a previously-developed approach for the study of isolated LOX droplets evaporating in hydrogen flows [1,19]. A unified treatment of general fluid thermodynamics and accurate calculations of transport properties, which are capable of treating fluid states over the entire thermodynamic regime, is combined with a preconditioning numerical scheme [32] for the present studies. This work focuses on the effects of droplet interactions on droplet dynamics and vaporization characteristics. Results obtained herein have practical implications and fundamental importance for modeling spray combustion in hydrogen/oxygen rocket engines.

2. Theoretical formulation

The physical model is concerned with two liquid oxygen (LOX) droplets moving and evaporating in tandem in a supercritical hydrogen stream, as shown in Fig. 1. The droplet temperature is initially uniform at a subcritical value, but the pressure and temperature of the ambient hydrogen are in the supercritical regime, for both oxygen and hydrogen. The critical properties of hydrogen and oxygen are listed in Table 1.

Once the two droplets are injected into the hydrogen environment, their surface heats up and reaches the thermodynamic critical mixing state almost instantaneously, due to the cryogenic fluid properties of oxygen and efficient energy transfer from the surrounding fluid [13,17]. The enthalpy of vaporization and surface tension vanish. Although the droplet interior remains at liquid state with a subcritical temperature (the compressibility factor is around 0.346 at 100 K and 100 atm), the entire flowfield, including both the oxygen droplets and surrounding hydrogen, becomes essentially a continuous medium without well-defined liquid/gas interfacial boundaries. The droplet can be conveniently defined as a dense fluid pocket enclosed by a surface that attains the critical mixing temperature [13,17,19], as listed in Table 2. A single-phase supercritical fluid model is thus employed in the present study [19].

The flowfield is treated as laminar and axisymmetric in the present study because of the low-Reynolds-number conditions. The conservation equations of mass, momentum, energy, and species concentrations can be presented in the following vector form:

$$\frac{\partial Q}{\partial t}+\frac{\partial (E-E_v)}{\partial x}+\frac{\partial (F-F_v)}{\partial r}=S \tag{1}$$

where the dependent variables are expressed as

$$Q=r[\rho \quad \rho u_x \quad \rho u_r \quad \rho e_t \quad \rho Y_i]^T \tag{2}$$

In Eq. (1), the convective flux vectors in the axial and radial directions are

$$E=r\begin{bmatrix}\rho u_x\\ \rho u_x^2+p\\ \rho u_x u_r\\ (\rho e_t+p)u_x\\ \rho u_x Y_i\end{bmatrix} \tag{3}$$

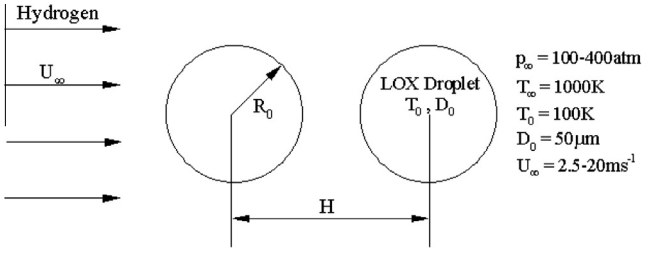

Fig. 1. Two liquid oxygen (LOX) droplets in tandem in supercritical convective hydrogen stream.

Table 1
Critical properties of oxygen and hydrogen.

	Oxygen	Hydrogen
p_c (MPa)	5.043	1.296
T_c (K)	154.58	33.15

Table 2
Critical mixing temperature of hydrogen/oxygen system.

Pressure (atm)	Critical mixing temperature (K)
100	142.8
200	127.2
400	116.0

$$F = r\begin{bmatrix} \rho u_r \\ \rho u_x u_r \\ \rho u_r^2 + p \\ (\rho e_t + p)u_r \\ \rho u_r Y_i \end{bmatrix} \tag{4}$$

The diffusive flux vectors are

$$E_v = r\begin{bmatrix} 0 \\ \tau_{xx} \\ \tau_{xr} \\ u_x\tau_{xx} + u_r\tau_{xr} - q_x \\ -\rho\hat{u}_{x,i}Y_i \end{bmatrix} \tag{5}$$

$$F_v = r\begin{bmatrix} 0 \\ \tau_{xr} \\ \tau_{rr} \\ u_x\tau_{xr} + u_r\tau_{rr} - q_r \\ -\rho\hat{u}_{r,i}Y_i \end{bmatrix} \tag{6}$$

The source term arises from the axisymmetric geometry and can be expressed as

$$S = \begin{bmatrix} 0 \\ -\frac{\partial}{\partial x}\left(\frac{2}{3}\mu u_r\right) \\ p - \frac{4}{3}\frac{\mu u_r}{r} + \frac{2}{3}\mu\frac{\partial u_x}{\partial x} - \frac{2}{3}u_r\frac{\partial \mu}{\partial r} \\ -\frac{\partial}{\partial x}\left(\frac{2}{3}\mu u_x u_r\right) - \frac{\partial}{\partial r}\left(\frac{2}{3}\mu u_r^2\right) \\ 0 \end{bmatrix} \tag{7}$$

Standard notation in fluid mechanics is used in these equations; terms are defined in the nomenclature. More details concerning these equations can be found in Refs. [19,32].

Accurate estimation of thermophysical properties is a prerequisite in the study of high-pressure transport phenomena. In our earlier work, a general framework has been established for property evaluations. An extended corresponding-state method is employed to calculate transport properties of a fluid mixture, including viscosity and thermal conductivity [1,19]. Fundamental thermodynamics theories and the Soave–Redlich–Kwong (SRK) equation of state are employed to determine thermodynamic properties, including heat capacity and internal energy [32]. A simple corresponding-state approach has been implemented to take into account of the pressure effect on mass diffusivity [1,19].

The present supercritical fluid model is solved numerically using a dual time-stepping preconditioning algorithm combined with a unified treatment of general fluid thermodynamics [32]. The scheme further incorporates the above-mentioned property evaluation methods for accurately calculating strong property variations at supercritical pressures. The pressure, species mass fractions, and enthalpy are obtained directly by solving the conservation equations. The temperature is calculated iteratively, based on the variables from the conservation equations and thermodynamic properties from the SRK equation of state [32]. The overall numerical framework and property-evaluation methods have been verified and experimentally validated against a number of test problems involving droplet vaporization in quiescent environments [13,17,32], supercritical jet dynamics and combustion phenomena [33–36], and heat transfer of hydrocarbon fuels at supercritical pressures [37–39].

3. Results and discussions

The theoretical model and numerical scheme outlined in the preceding section have been applied to study the interaction and vaporization of a pair of LOX droplets in convective hydrogen streams at supercritical pressures. As shown schematically in Fig. 1, at $t = 0$ μs, droplets are suddenly released into the hydrogen stream. The initial diameter and temperature of the droplets are 50 μm and 100 K, respectively, and the ambient hydrogen temperature is taken to be 1000 K. A wide range of ambient pressure (100–400 atm) and freestream velocity (2.5–20 m/s) are considered. The initial droplet spacing, H, is prescribed, and the ratio of the initial droplet spacing and droplet radius, H/R, is used to indicate the intensity of droplet interaction. The present work is limited to laminar axisymmetric flows. The freestream Reynolds number based on the initial droplet diameter ($\mathrm{Re} = u_\infty D_0/\nu_\infty$) is less than 300.

Although the droplet temperature is initially at a subcritical state, the droplet surface reaches its thermodynamic critical mixing point almost instantaneously upon introduction to the hydrogen stream [1,13,17]. Once this occurs, the enthalpy of vaporization and surface tension vanish, and the subsequent vaporization process becomes diffusion and convection controlled. Since thermal transport proceeds at a rate faster than mass transfer for hydrogen/oxygen systems at supercritical pressures, no hydrogen can penetrate inside the oxygen droplet [19].

3.1. Flow development

The flowfields around the leading and trailing droplets are considerably different. Figs. 2–4 present the flow development with different H/R ratios at an ambient pressure of 100 atm. The freestream velocity is 20 m/s and the corresponding Reynolds number is $\mathrm{Re} \approx 120$. Streamlines are used to show the instant flowfields, while the temperature distributions indicate the droplet vaporization behaviors.

Fig. 2 shows the situation with an H/R ratio of 4. At the beginning of the vaporization process, a small recirculating eddy develops in the wake of each droplet. Since the leading droplet faces a stronger incoming flow, the associated flow separation occurs earlier and results in a slightly larger recirculating region. At $t = 40$ μs, the leading droplet forms a disk-like shape, which further enhances flow separation and produces a much larger recirculating zone behind the droplet. The distance between the two droplets then decreases, and the trailing droplet tends to push the leading recirculating eddy upwards. Although the trailing recirculating eddy also grows during this process, it remains small compared with the leading eddy.

When the leading droplet moves further closer to the trailing droplet at $t = 65$ μs, the leading recirculating eddy is lifted to the top of the trailing droplet and decreases in size because the free space is limited. At this instant, the two recirculation zones are essentially in touch with each other. As time elapses to $t = 85$ μs, the two droplets start to interact closely, and their combined effect

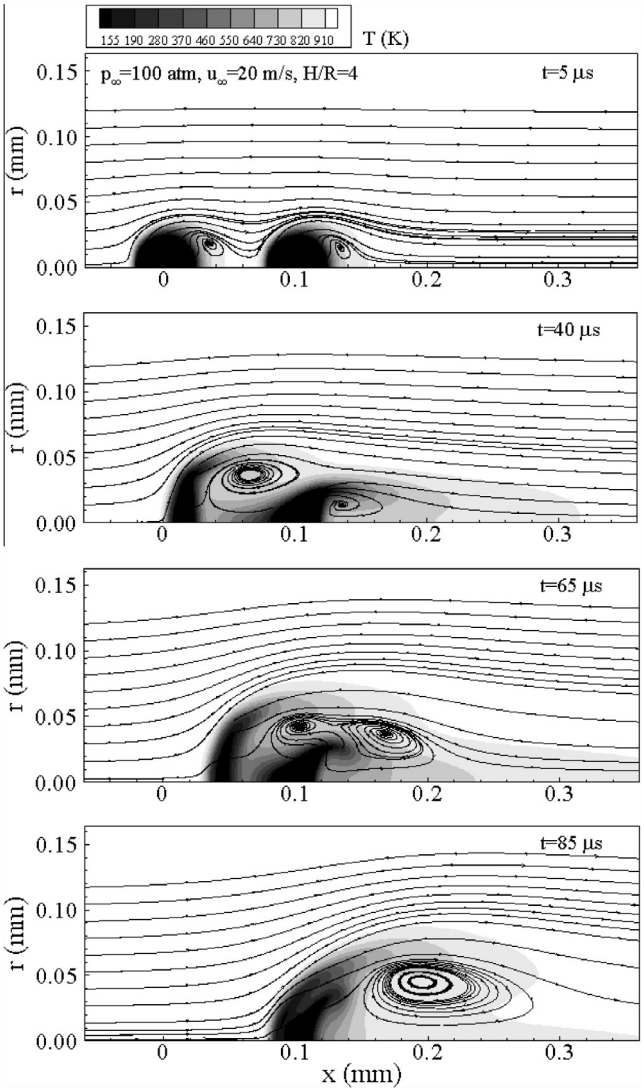

Fig. 2. Flow and droplet evolution at ambient pressure of 100 atm, incoming velocity of 20 m/s, and H/R ratio of 4.

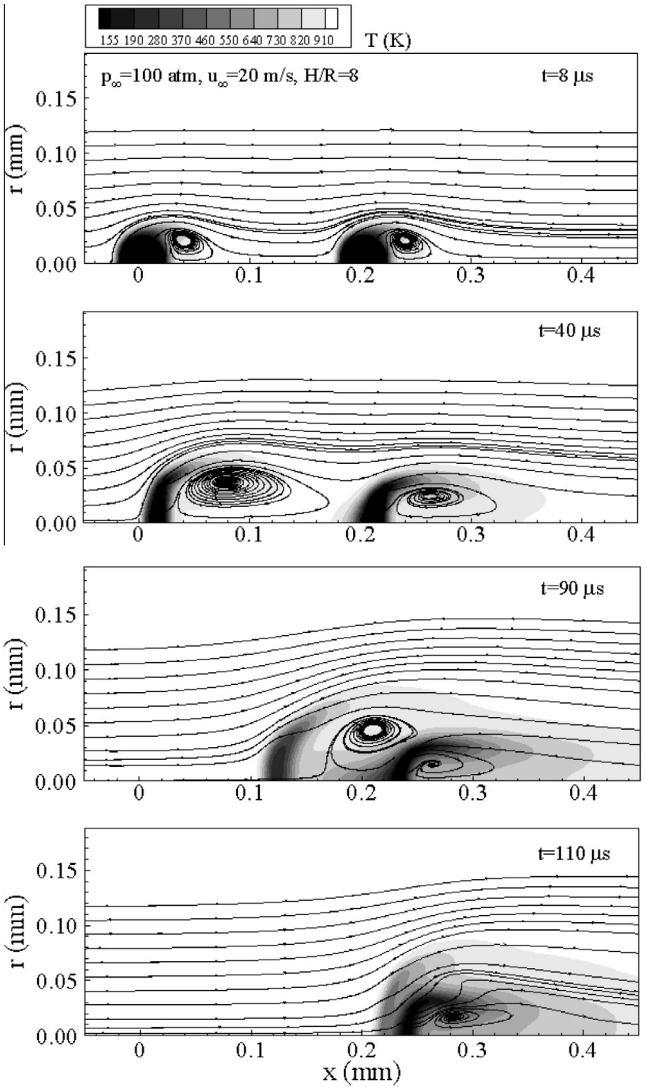

Fig. 3. Flow and droplet evolution at ambient pressure of 100 atm, incoming velocity of 20 m/s, and H/R ratio of 8.

on the flowfield becomes similar to that of an isolated droplet. In the meantime, the two recirculating eddies merge and produce a single large recirculating zone.

Fig. 3 shows the flow evolution with an H/R ratio of 8. Initially, two independent recirculating eddies form and develop behind their respective droplets. As time elapses, the leading eddy grows much faster than the trailing one, for two reasons. First, the deformation of the leading droplet promotes flow separation. Second, the presence of the trailing droplet affects the flow development behind the leading one and thus further enhances flow separation. Once the two droplets move closer, the leading recirculating eddy is pushed upwards and decreases in size. The size of the trailing eddy decreases as well, mainly because of the backward deformation of the trailing droplet. At $t = 110$ μs, the remaining mass from the leading droplet merges with the trailing droplet and gives rise to a single, larger recirculating zone.

As the H/R ratio increases to 12, the interaction between the two droplets becomes weak, as shown in Fig. 4. The leading recirculating eddy continues to grow through the entire vaporization process, mainly due to the droplet deformation and enhanced flow separation promoted by the trailing droplet. The trailing recirculating eddy increases in size at the beginning of the vaporization process, but decreases gradually in the late stages because of the backward deformation of the trailing droplet, which eases flow separation.

3.2. Temperature field

Figs. 5 and 6 show the droplet evolution with two different H/R ratios at an ambient pressure of 100 atm. The freestream velocity is 10 m/s. At $H/R = 4$, the two droplets evaporate independently in the early stage. Droplet interaction soon occurs and gradually dictates the vaporization process. At $t = 60$ μs, the two droplets behave in completely different patterns. The leading droplet deforms perpendicular to the flow direction and retains a crescent shape, influenced mainly by the strong incoming flow and the presence of the trailing droplet. A large recirculating region takes place behind the droplet, as shown in Figs. 2 and 3. The deformation of the trailing droplet, influenced by the leading droplet and a much weaker incoming flow, is controlled mainly by the diffusion process. This phenomenon is especially profound near the axisymmetric axis, where the trailing droplet expands strongly in both the downstream and upstream directions. As time elapses to 155μs, the droplets move very close to each other. The leading droplet starts to break up from its core. Since the droplet mass is moving toward

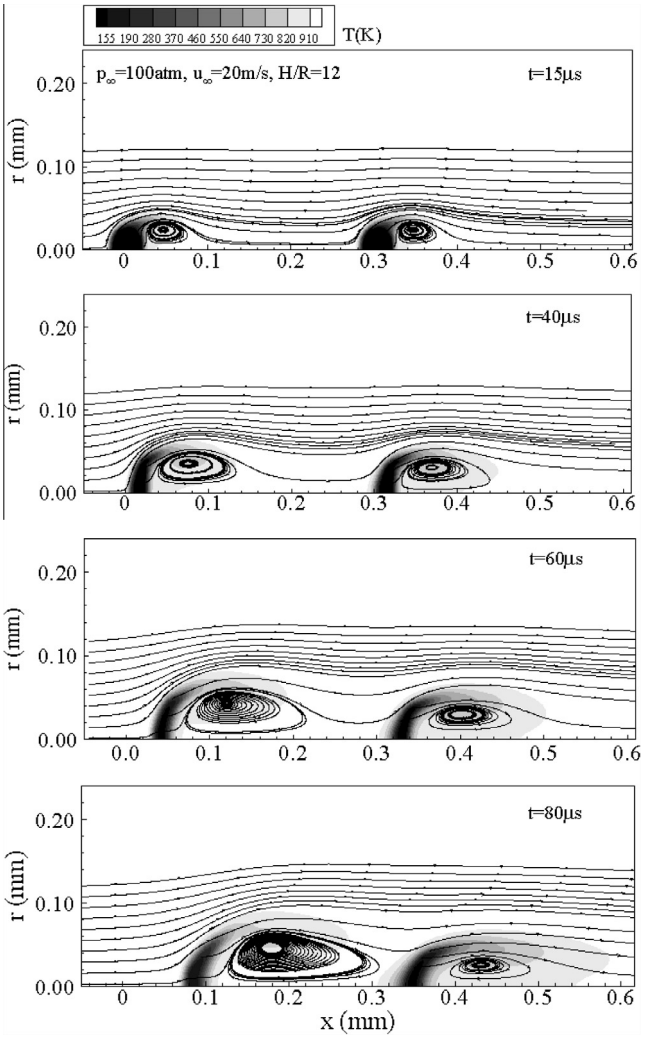

Fig. 4. Flow and droplet evolution at ambient pressure of 100 atm, incoming velocity of 20 m/s, and H/R ratio of 12.

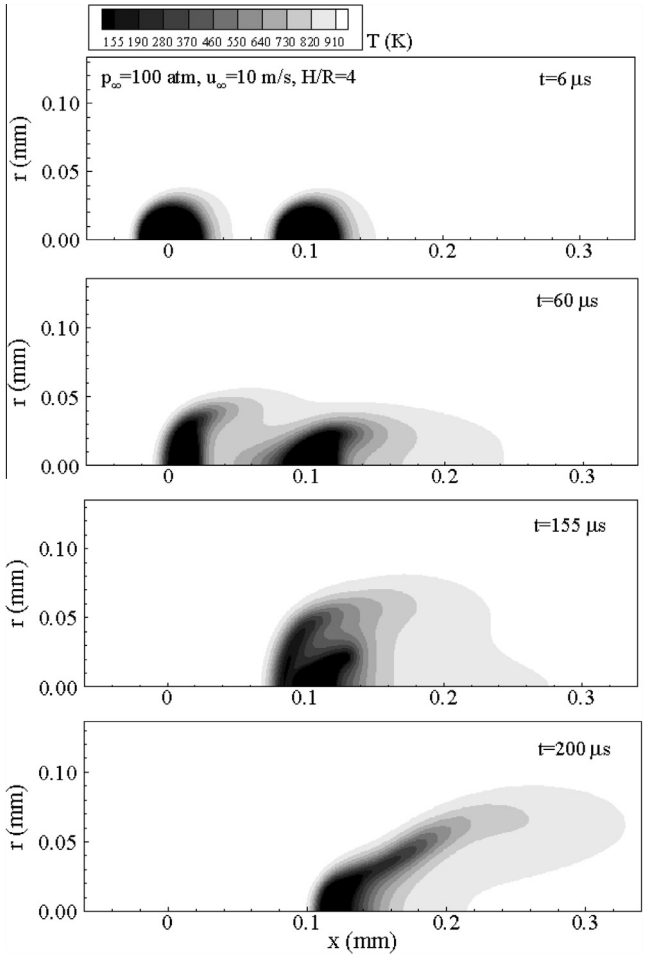

Fig. 5. Evolution of the temperature field at ambient pressure of 100 atm, incoming velocity of 10 m/s, and H/R ratio of 4.

the edge after break-up, this can be considered the typical forward bag-type break-up [40,41]. The separated mass is carried downstream over the surface of the trailing droplet. Once the remaining mass of the leading droplet merges into its trailing counterpart, the resultant LOX pocket starts to behave as an isolated droplet. It then directly confronts the free stream, and a significant stretching is clearly seen at $t = 200$ μs.

Fig. 6 shows the situation with $H/R = 8$. At $t = 145$ μs, the leading droplet expands considerably, perpendicular to the centerline, and takes on a slightly convex disk shape. In the meantime, the trailing droplet is bent downstream and exhibits a skirt-like shape. As time continues to $t = 190$ μs, the leading droplet evaporates completely before the two droplets come into contact. No break-up is observed for the leading droplet in the course of the vaporization process, because of the smaller Reynolds number and reduced droplet interaction. It should be noted that the droplet surface is defined at the critical mixing temperature in the present study, as listed in Table 2. The present result is consistent with that for a single droplet [19], for which it was found that a dimensionless parameter, representing the ratio of the aerodynamic to viscous force, dictates droplet deformation under supercritical conditions. Droplet break-up becomes difficult without the influence of surface tension and assistance of a neighboring droplet, especially at low Reynolds-number conditions. For large droplet spacing with H/R ratio greater than 12 (not shown), the two droplets both behave like isolated droplets during the vaporization process, mainly deforming perpendicular to the centerline. Detailed discussion of deformation of an isolated droplet can be found in our prior publication [19].

Droplet interaction becomes weaker with increasing ambient pressure. For example, at an ambient pressure of 400 atm and an incoming velocity of 10 m/s, the two droplets act as isolated entities when the H/R ratio is greater than 8, as opposed to 12 at 100 atm. At a higher ambient pressure, because of the increased hydrogen density, the hydrogen stream contains more energy. Therefore, the effects of droplet vaporization on the temperature field become weak. Moreover, the denser hydrogen between the two droplets affects the flow development, preventing the two droplets from moving closer.

3.3. Mass fraction field

Figs. 7 and 8 show the evolution of the mass-fraction field, with the flow conditions corresponding to those for Figs. 5 and 6, respectively. For small droplet spacing of $H/R = 4$, the leading LOX droplet starts to vaporize and diffuse downstream because of strong convection, soon after being introduced to the hydrogen flow. At $t = 60$ μs, the mass-fraction field behaves very much like the temperature field shown in Fig. 5. As time continues to $t = 125$ μs, the two droplets collide and merge to produce a mush-

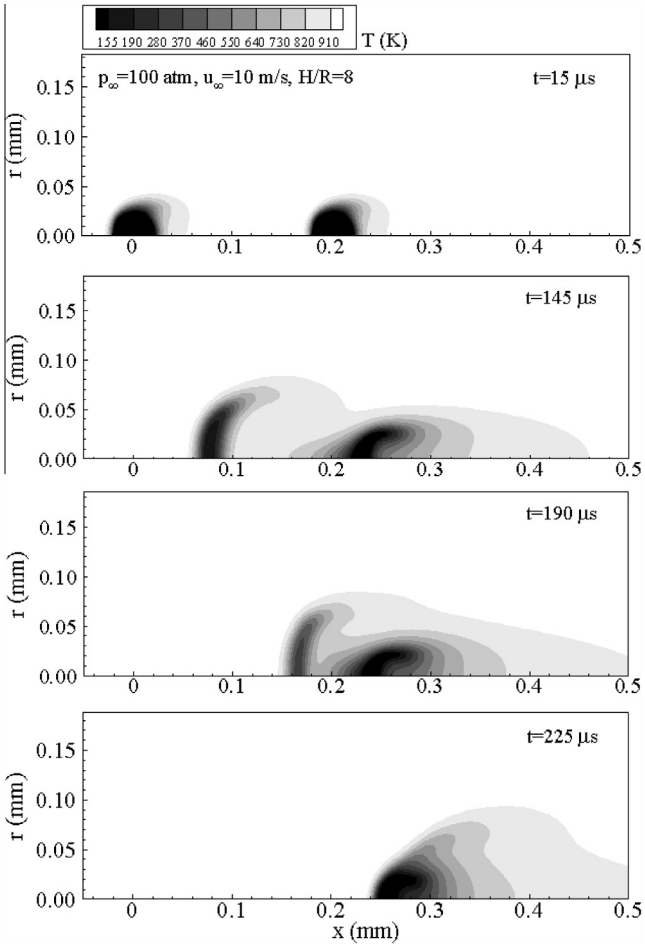

Fig. 6. Evolution of the temperature field at ambient pressure of 100 atm, incoming velocity of 10 m/s, and H/R ratio of 8.

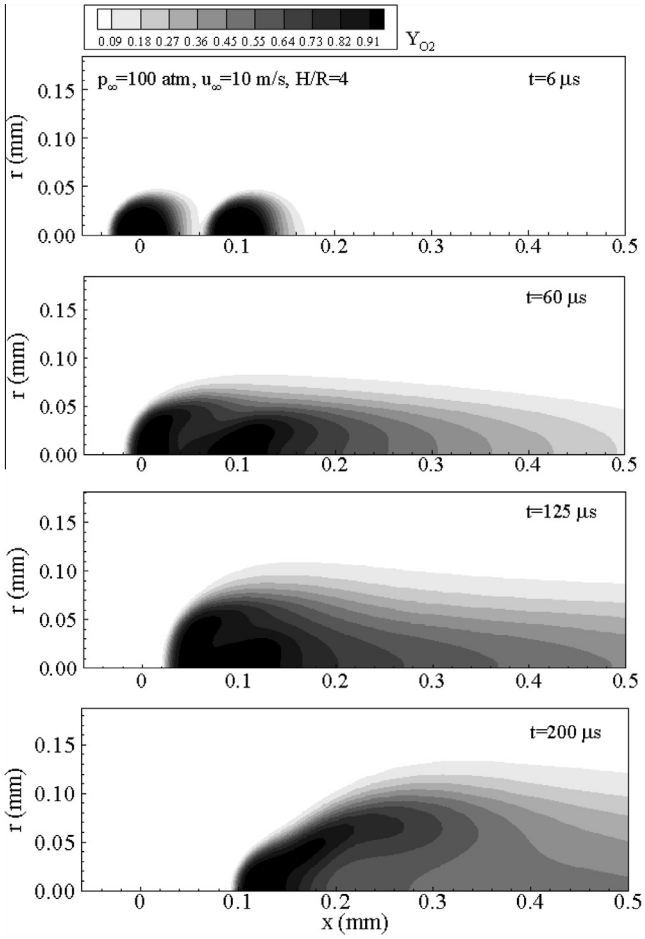

Fig. 7. Evolution of the oxygen concentration field at ambient pressure of 100 atm, incoming velocity of 10 m/s, and H/R ratio of 4.

room-like shape. This feature is drastically different from the corresponding temperature field, a phenomenon that can be attributed to the large disparity between the mass and thermal transfer [19]. In addition, no forward bag-type break-up is observed for the leading droplet in the mass fraction field. At the end of the vaporization process, the two droplets completely merge and behave like an isolated droplet.

Fig. 8 shows the situation with $H/R = 8$. No droplet interaction is found up to 15 μs. At $t = 60$ μs, the oxygen-rich region extending from the leading droplet is in touch with that from the trailing droplet, due to the strong convective transport. The coupling between droplets, however, is limited, and the two droplets undergo similar deformation independently. At $t = 190$ μs, the two droplets coalesce. The leading droplet expands strongly, perpendicular to the flow direction, while the trailing droplet is mainly stretched along the flow direction. Finally, at $t = 225$ μs, the two droplets completely merge into a single droplet, which is slightly stretched at the tip. The deformation of this resultant droplet is different from that of an isolated droplet, which retains a crescent shape at the end of the vaporization process [19].

Droplet interaction in terms of the mass fraction field becomes extremely weak as the H/R ratio increases to 12. Both droplets behave like isolated droplets and retain their crescent shapes at the end of the vaporization process. As in the evolution of the temperature field, an increase in the pressure from 100 to 400 atm significantly weakens droplet interaction, which essentially disappears when the H/R ratio exceeds 8 at 400 atm.

3.4. Droplet lifetime and trajectory

The vaporization rates and lifetimes of the two droplets are examined with different ambient pressures (100 and 400 atm) and initial droplet spacings ($H/R = 4$–12). The droplet is defined by the critical mixing temperature. Fig. 9 shows the results. Only minor effects on the vaporization of the leading droplet are observed, whereas major impact occurs with the trailing droplet. As shown in Fig. 9(a), the two droplets evaporate at a same rate only at the beginning stage of the vaporization process, because there is a sharp temperature gradient at the droplet surface when the two droplets are suddenly introduced into the high-temperature hydrogen streams. The vaporization rate of the trailing droplet starts to decrease quickly, but the exact deviation point depends on the droplet spacing. For $H/R = 4$, the vaporization rate of the trailing droplet slows down shortly after the vaporization process begins. Around 90–100 μs, when the leading droplet breaks up, the vaporization rate of the trailing droplet experiences the second major change. During this time period, the leading droplet mass (after break-up) is carried over the surface of the trailing droplet, thus significantly affecting its vaporization rate. No second transition exists in the other two cases with $H/R = 8$ and 12, due to the lack of the break-up of the leading droplet.

Fig. 9(b) shows the vaporization rates of the two interacting droplets at an ambient pressure of 400 atm. The droplet Reynolds number ($Re \approx 120$) remains identical to that shown in Fig. 9(a). The corresponding free stream velocity is 5 m/s. Under such a high pressure, the effect of droplet interaction becomes extremely

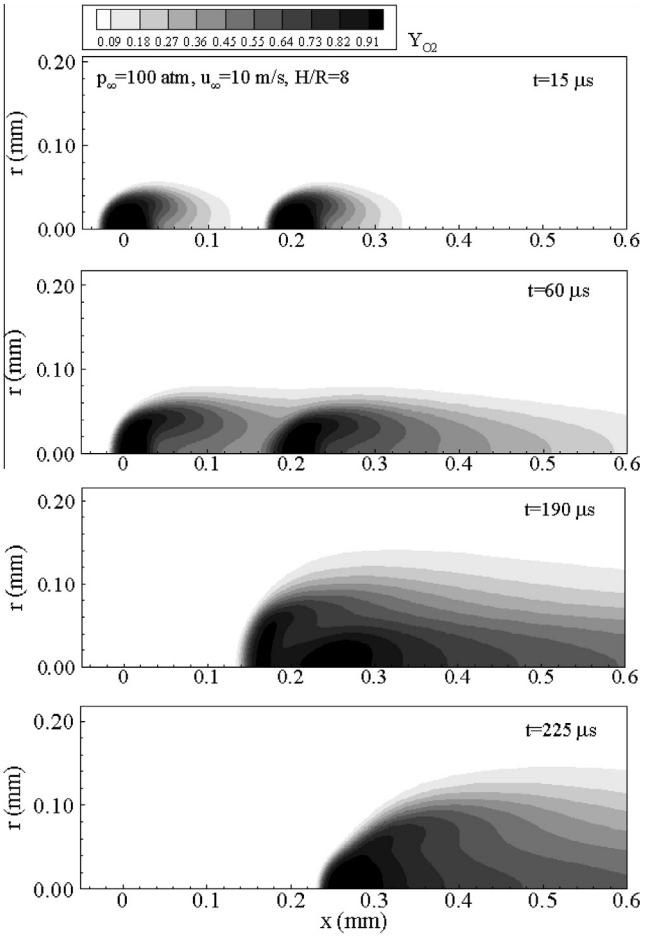

Fig. 8. Evolution of the oxygen concentration field at ambient pressure of 100 atm, incoming velocity of 10 m/s, and H/R ratio of 8.

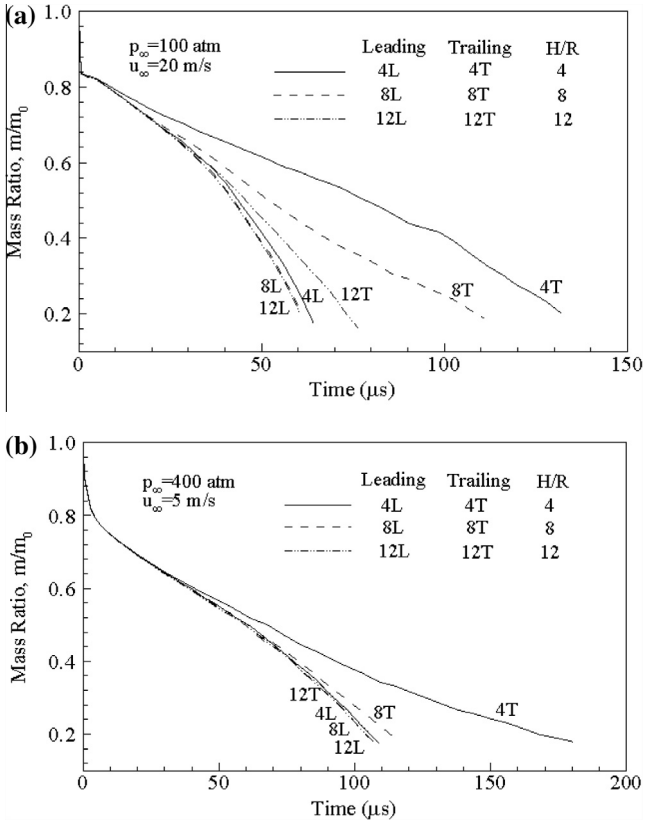

Fig. 9. Vaporization rates of the leading and trailing droplets: (a) ambient pressure of 100 atm and incoming velocity of 20 m/s, and (b) ambient pressure of 400 atm and incoming velocity of 5 m/s.

weak. Discernible change of the vaporization rate of the trailing droplet occurs only when the two droplets are closely placed, with an H/R ratio of 4 or less.

To better understand the effect of droplet interaction on the vaporization rate, the lifetimes of the leading and trailing droplets are compared with that of an isolated droplet under the same operating conditions. A droplet lifetime ratio, τ, is thus defined as

$$\tau = \frac{\textit{lifetime of an isolated droplet}}{\textit{lifetime of the leading or trailing droplet}} \tag{8}$$

where the lifetime of an isolated droplet is obtained as a function of the initial Reynolds number and ambient pressure in our previous study [19].

Fig. 10 shows the variations of the droplet lifetime ratios at different ambient pressures and incoming velocities. At a pressure of 100 atm, as shown in Fig. 10(a), droplet interaction produces only a minor effect on the lifetime of the leading droplet, with a droplet lifetime ratio of around 0.8 for $H/R = 4$. The lifetime of the trailing droplet is, however, substantially prolonged under the influence of the leading droplet. The droplet lifetime ratio decreases to around 0.5 with the same H/R ratio.

As shown in Fig. 10(b), increasing the ambient pressure significantly weakens the effect of interaction on droplet lifetimes, especially for large droplet spacing. For example, at 400 atm, the lifetime ratios of the trailing and leading droplets exceed 0.8 and 0.9, respectively, for $H/R = 8$. Results also indicate that the ambient pressure exerts much stronger influences on the lifetimes of the two interacting droplets than does the free stream velocity.

For droplets vaporizing in a supercritical, forced-convective environment, the total drag force consists of form, friction, and thrust drags, of which the form drag is usually the dominant component [19]. Fig. 11(a) shows the trajectories of the mass centers of the two droplets, in reference to their respective initial locations, at three different H/R ratios. The ambient pressure is 100 atm, and the freestream velocity is 20 m/s. The trailing droplet exerts a minor effect on the motion of the leading droplet, whose trajectory is comparable to that of an isolated droplet [19]. The situation for the trailing droplet, however, is considerably different for droplet spacing of $H/R = 4$. Its trajectory deviates from that of the leading droplet shortly after vaporization takes place, and the droplet moves slowly thereafter. From $t = 50$ μs on, the droplet shows a slight forward movement, dictated by the form drag. After $t = 90$ μs, when the leading droplet breaks up, the trailing droplet starts to move like an isolated droplet. For $H/R = 8$, a transition period exists, during which the movement of the trailing droplet slows tremendously, but no forward droplet movement is observed.

Fig. 11(b) shows droplet trajectories at an ambient pressure of 400 atm and a free stream velocity of 5 m/s. The Reynolds number ($\mathrm{Re} \approx 120$) remains identical to the case shown in Fig. 11(a). Under this condition, the trajectories between the leading and trailing droplets differ significantly only for small droplet spacing (H/R ratio less than 4). This observation is consistent with the preceding conclusion that high pressure produces weak droplet interaction. At $H/R = 4$, a transition time for the trailing droplet starts at about 100 μs. Afterwards, the trailing droplet moves very slowly through the end of the vaporization process. No forward droplet movement is observed in the cases studied at 400 atm.

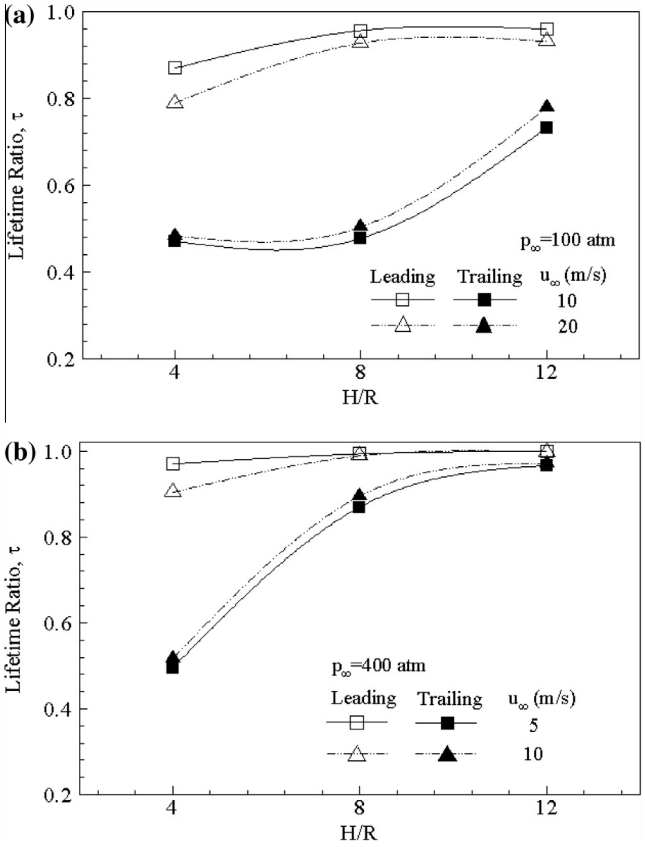

Fig. 10. Droplet lifetime ratios of the leading and trailing droplets: (a) ambient pressure of 100 atm, and (b) ambient pressure of 400 atm.

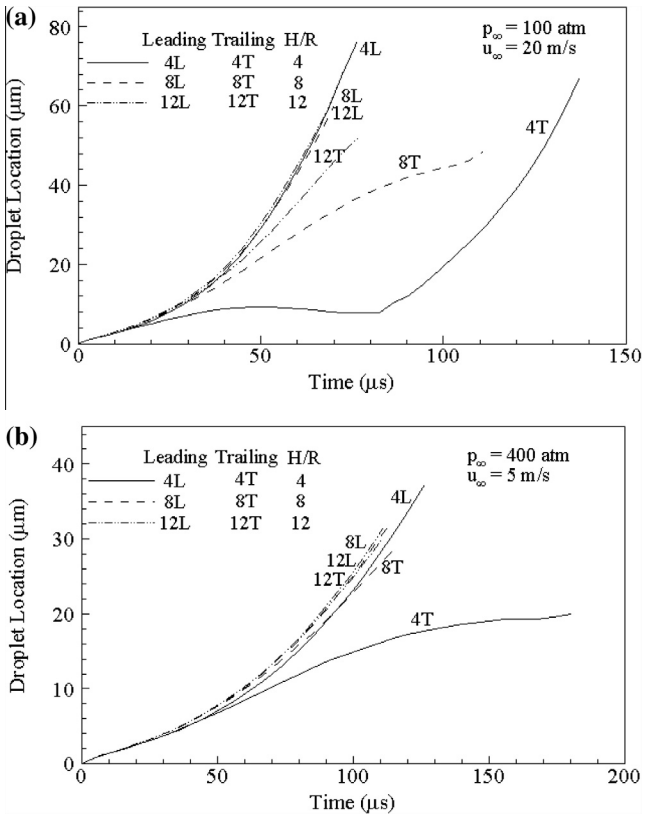

Fig. 11. Trajectories of the leading and trailing droplets: (a) ambient pressure of 100 atm and incoming velocity of 20 m/s, and (b) ambient pressure of 400 atm and incoming velocity of 5 m/s.

4. Conclusions

Interaction and vaporization of two liquid oxygen (LOX) droplets in tandem in forced convective hydrogen environments have been numerically investigated over a range of supercritical pressures between 100–400 atm, freestream velocities from 2.5 to 20 m/s, and spacing ratios of $H/R = 4–12$. The theoretical framework accommodates a complete set of conservation equations of mass, momentum, energy, and species concentrations. The numerical solution is based on a unified treatment of general fluid thermodynamics integrated into a dual time-stepping preconditioning approach. The scheme also incorporates self-consistent evaluation methods for accurate calculations of thermophysical properties over the range of fluid states of concern.

The present study focuses on the effects of droplet interaction on the dynamics and vaporization characteristics of each constituent droplet. Droplet interaction strongly affects the flow development around the two LOX droplets. A forward bag-type break-up of the leading droplet is observed when the two droplets are initially placed close together at an H/R ratio of 4 and an ambient pressure of 100 atm. As the droplet spacing increases, the interaction weakens. The leading droplet, which is confronted with the strong incoming stream and influenced by the trailing droplet, mainly deforms perpendicular to the flow direction, while the trailing droplet deforms primarily in the streamwise direction.

The trailing droplet produces only minor effects on the vaporization lifetime and moving dynamics of the leading droplet. In contrast, with the presence of the leading droplet, the lifetime of the trailing droplet is substantially prolonged and its moving trajectory is strongly altered. A forward movement is observed for the trailing droplet at an H/R ratio of 4 and an ambient pressure of 100 atm. Increasing ambient pressure weakens droplet interaction. This conclusion is verified in terms of flowfield development and droplet vaporization behaviors.

Acknowledgments

This work was sponsored by the William R.T. Oakes Endowment at the Georgia Institute of Technology, the US Air Force Office of Scientific Research (AFOSR) under Grant No. F49620-01-1-0114, and the Zhejiang Provincial Natural Science Foundation of China (R1100300). The support and encouragement from Dr. Mitat Birkan of AFOSR is gratefully acknowledged.

References

[1] V. Yang, Modeling of supercritical vaporization, mixing, and combustion processes in liquid-fueled propulsion systems, Proc. Combust. Inst. 28 (2001) 925.
[2] K.C. Hsieh, J.S. Shuen, V. Yang, Droplet vaporization in high-pressure environments. I: Near critical conditions, Combust. Sci. Technol. 76 (1991) 111.
[3] J.S. Shuen, V. Yang, G.C. Hsiao, Combustion of liquid-fuel droplet in supercritical conditions, Combust. Flame 89 (1992) 299.
[4] J.P. Delplanque, W.A. Sirignano, Numerical study of the transient vaporization of an oxygen droplet at sub- and super-critical conditions, Int. J. Heat Mass Transfer 36 (1993) 303.
[5] V. Yang, N.N. Lin, J.S. Shuen, Vaporization of liquid oxygen (LOX) droplets in supercritical hydrogen environments, Combust. Sci. Technol. 97 (1994) 247.
[6] H. Nomura, Y. Ujiie, H.J. Rath, J. Sato, M. Kono, Experimental study on high pressure droplet evaporation using microgravity conditions, Proc. Combust. Inst. 26 (1996) 1267.
[7] K. Harstad, J. Bellan, Isolated fluid oxygen drop behavior in fluid hydrogen at rocket chamber pressures, Int. J. Heat Mass Transfer 41 (1998) 3537.
[8] W.A. Sirignano, J.P. Delplanque, Transcritical vaporization of liquid fuels and propellants, J. Propul. Power 15 (1999) 896.
[9] C. Chauveau, I. Gökalp, D. Segawa, T. Kadota, H. Enomoto, Effects of reduced gravity on methanol droplet combustion at high pressures, Proc. Combust. Inst. 28 (2001) 1071.
[10] G.S. Zhu, R.D. Reitz, A model for high-pressure vaporization of droplets of complex liquid mixtures using continuous thermodynamics, Int. J. Heat Mass Transfer 45 (2002) 495.

[11] C. Yan, S.K. Aggarwal, A high-pressure droplet model for spray simulations, J. Eng. Gas Turbine Power 128 (2006) 482.
[12] J.H. Bae, C.T. Avedisian, High-pressure combustion of submillimeter-sized nonane droplets in a low convection environment, Combust. Flame 145 (2006) 607.
[13] P. Lafon, H. Meng, V. Yang, M. Habiballah, Vaporization of liquid oxygen (LOX) droplets in hydrogen and water environments under sub- and super-critical conditions, Combust. Sci. Technol. 180 (2008) 1.
[14] G.C. Hsiao, H. Meng, V. Yang, Pressure-coupled vaporization response of n-pentane fuel droplet at subcritical and supercritical conditions, Proc. Combust. Inst. 33 (2011) 1997.
[15] T.L. Jiang, W.T. Chiang, Effects of multiple droplet interaction on droplet vaporization in subcritical and supercritical pressure environments, Combust. Flame 97 (1994) 17.
[16] K. Harstad, J. Bellan, Interactions of fluid oxygen drops in fluid hydrogen at rocket chamber pressures, Int. J. Heat Mass Transfer 41 (1998) 3551.
[17] H. Meng, V. Yang, Clustering effects of liquid oxygen (LOX) droplet vaporization in hydrogen environments at subcritical and supercritical pressures, Int. J. Hydrogen Energy 37 (2012) 11815.
[18] J. Daou, B. Rogg, Convective burning of gaseous fuel pockets and supercritical droplets, Combust. Flame 115 (1998) 145.
[19] H. Meng, G.C. Hsiao, V. Yang, J.S. Shuen, Transport and dynamics of liquid oxygen droplets in supercritical hydrogen streams, J. Fluid Mech. 527 (2005) 115.
[20] H. Zhang, V. Raghavan, G. Gogos, Subcritical and supercritical droplet evaporation within a zero-gravity environment: low Weber number relative motion, Int. Commun. Heat Mass Transfer 35 (2008) 385.
[21] M. Birouk, M.M. Abou Al-Sood, Droplet evaporation in a turbulent high-pressure freestream, Int. J. Therm. Sci. 49 (2010) 264.
[22] B. Balaji, V. Raghavan, K. Ramamurthi, G. Gogos, A numerical study of evaporation of spherical n-dodecane droplets in high pressure nitrogen environment, Phys. Fluids 23 (2011) 063601.
[23] N. Chigier, Optical imaging sprays, Prog. Energy Combust. Sci. 17 (1991) 211.
[24] C.S. Connon, D. Dunn-Rankin, Droplet stream dynamics at high ambient pressure, Atomization Sprays 6 (1996) 485.
[25] V. Deprédurand, G. Castanet, F. Lemoine, Heat and mass transfer in evaporating droplets in interaction: influence of the fuel, Int. J. Heat Mass Transfer 53 (2010) 3495.
[26] M.S. Raju, W.A. Sirignano, Interaction between two vaporizing droplets in an intermediate Reynolds number flow, Phys. Fluids A 2 (1990) 1780.
[27] C.H. Chiang, M.S. Raju, W.A. Sirignano, Numerical analysis of convecting, vaporizing fuel droplet with variable properties, Int. J. Heat Mass Transfer 35 (1992) 1307.
[28] C.H. Chiang, W.A. Sirignano, Interacting, convecting, vaporizing fuel droplets with variable properties, Int. J. Heat Mass Transfer 36 (1993) 875.
[29] B. Frackowiak, G. Lavergne, C. Tropea, A. Strzelecki, Numerical analysis of the interactions between evaporating droplets in a monodisperse stream, Int. J. Heat Mass Transfer 53 (2010) 1392.
[30] C.P. Cho, H.Y. Kim, S.S. Yoon, Interacting of the burning spherical droplets in oxygen-enriched turbulent environment, Combust. Flame 156 (2009) 14.
[31] M. Birouk, C. Chauveau, I. Gökalp, Turbulence effects on the combustion of single hydrocarbon droplets, Proc. Combust. Inst. 28 (2000) 1015.
[32] H. Meng, V. Yang, A unified treatment of general fluid thermodynamics and its application to a preconditioning scheme, J. Comput. Phys. 189 (2003) 277.
[33] N. Zong, H. Meng, S.-Y. Hiesh, V. Yang, A numerical study of cryogenic fluid injection and mixing under supercritical conditions, Phys. Fluids 16 (2004) 4248.
[34] N. Zong, V. Yang, Cryogenic fluid jets and mixing layers in transcritical and supercritical environments, Combust. Sci. Technol. 178 (2006) 193.
[35] N. Zong, V. Yang, Near-field flow and flame dynamics of LOX/methane shear coaxial injector under supercritical conditions, Proc. Combust. Inst. 31 (2007) 2309.
[36] Y. Yin, X. Lu, Effects of injection temperature on the jet evolution under supercritical conditions, Chin. Sci. Bull. 54 (2009) 4197.
[37] Y.-X. Hua, Y.-Z. Wang, H. Meng, A numerical study of supercritical forced convective heat transfer of n-heptane inside a horizontal miniature tube, J. Supercrit. Fluids 52 (2010) 36.
[38] Y.Z. Wang, Y.-X. Hua, H. Meng, Numerical studies of supercritical turbulent convective heat transfer of cryogenic-propellant methane, J. Thermophys. Heat Transfer 24 (2010) 490.
[39] B. Ruan, H. Meng, Supercritical heat transfer of cryogenic-propellant methane in rectangular engine cooling channels, J. Thermophys. Heat Transfer 26 (2012) 313.
[40] L.P. Hsiang, G.M. Faeth, Near-limit drop deformation and secondary breakup, Int. J. Multiphase Flow 18 (1992) 635.
[41] M. Pilch, C.A. Erdman, Use of breakup time data and velocity history data to predict the maximum size of stable fragments for acceleration-induced breakup of a liquid drop, Int. J. Multiphase Flow 13 (1987) 741.